J. Biomed. Eng. Res : 122-131, 2008

Speckle Noise Reduction and Edge Enhancement in Ultrasound Images Based on Wavelet Transform

Yong Sun Kim, Jong Beom Ra

School of Electrical Engineering & Computer Science, Korea Advanced Instituteof Science and Technology

(Received October 5, 2007. Accepted February 18, 2008)

Abstract

For B-mode ultrasound images, we propose an image enhancement algorithm based on a multi-resolution approach, which consists of edge enhancing and noise reducing procedures. Edge enhancement processing is applied sequentially to coarse-to-fine resolution images obtained from wavelet-transformed data. In each resolution, the structural features of each pixel are examined through eigen analysis. Then, if a pixel belongs to an edge region, we perform two-step filtering: that is, directional smoothing is conducted along the tangential direction of the edge to improve continuity and directional sharpening is conducted along the normal direction to enhance the contrast. In addition, speckle noise is alleviated by proper attenuation of the wavelet coefficients of the homogeneous regions at each band. This region-based speckle-reduction scheme is differentiated from other methods that are based on the magnitude statistics of the wavelet coefficients. The proposed algorithm enhances edges regardless of changes in the resolution of an image, and the algorithm efficiently reduces speckle noise without affecting the sharpness of the edge. Hence, compared with existing algorithms, the proposed algorithm considerably improves the subjective image quality without providing any noticeable artifacts.

Key words : ultrasound image enhancement, speckle-noise reduction, wavelet transform, eigen analysis, directional filtering

Ⅰ. INTRODUCTION

Ultrasound imaging has become a popular modality because it is safe, noninvasive, portable, relatively inexpensive, and has a real-time imaging capability. However, ultrasound images have a fundamental problem of poor quality, mainly caused by multiplicative speckle noise. Speckle noise, which is random mottling with bright and dark spots, obscures the fine details of an image and degrades the detectability of low-contrast lesions [1-4].

To reduce speckles, researchers have proposed a number of methods, such as temporal averaging, median filtering, homomorphic Wiener filtering, and adaptive spatial filtering [1-6]. Temporal averaging tries to increase the signal-to-noise ratio (SNR) by averaging the multiple uncorrelated images that are obtained by the transducer shift [1,4]. This method is good at reducing speckle noise but causes a loss of small details due to blurring. Homomorphic Wiener filtering converts multiplicative noise into additive noise and applies low-pass Wiener filtering. Adaptive weighted median filtering, which is an advanced version of median filtering, still has a limit to keep fine details in the image [5]. By using local features of image texture, adaptive spatial filtering performs low-pass filtering of speckle noise while preserving a resolved-object structure [6].

To reduce noise while preserving edges, other researchers have proposed more advanced filtering techniques based on anisotropic diffusion [7,8]. One recent method introduced the nonlinear coherent diffusion (NCD) model and proposed a Gaussian smoothing scheme based on the NCD model [8]. However, although the NCD model may be effective for finding edge pixels and their orientations in an ordinary image of homogeneous resolution, the NCD model fails to determine the resolution of a B-mode ultrasound image due to the imaging characteristics of such images [9,10].

Fig. 1 shows that a practical ultrasound image has a varying lateral resolution along the depth axis. For an image with an inhomogeneous resolution, edge detection based on the NCD model is inefficient because this method becomes sensitive to the noise of low resolution edges. Fig. 2 shows the problem of the NCD-based edge detection scheme for a phantom image; the image includes edges of various transition widths (or various resolutions) and white Gaussian noise. Fig. 2 also shows

Corresponding Author : Jong Beom Ra
School of Electrical Engineering & Computer Science, Korea Advanced Institute of Science and Technology, 335 Gwahangno, Yuseong-gu, Daejeon 305-701, Republic of Korea
Tel : +82-42-869-3434 / Fax : +82-42-869-8360
E-mail : jbra@ee.kaist.ac.kr

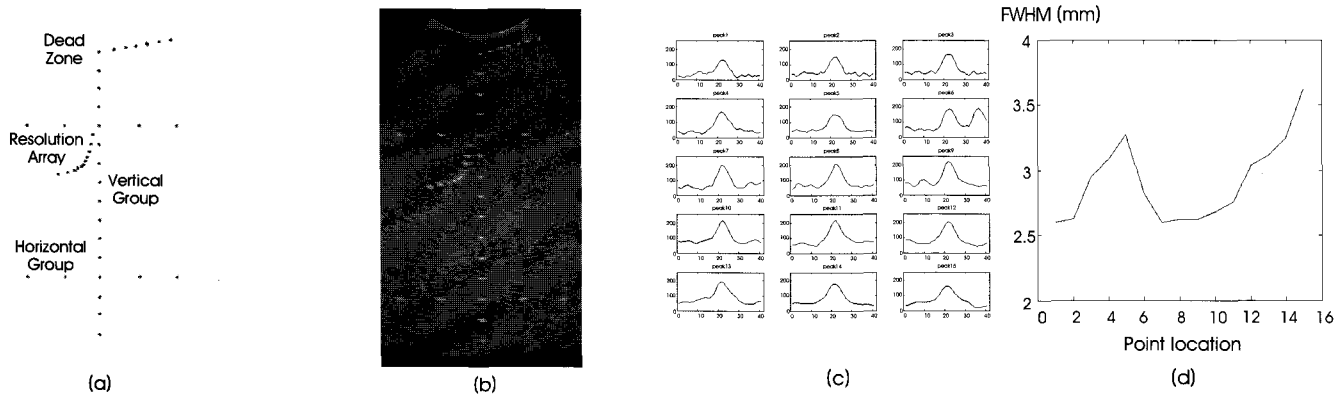

Fig. 1. (a) A resolution phantom of model 539, ATS Labs. (b) A corresponding ultrasound image. (c) Cut views along the lateral direction of vertically aligned points. (d) A full-width at half maximum, which represents the lateral resolution at each point.

that the NCD-based scheme has limited edge-detecting capabilities and is sensitive to noise.

In contrast to the single-resolution approach mentioned above, researchers have proposed various enhancement algorithms based on the multi-resolution approach [11-19]. Such algorithms generally use wavelet transform-based filtering, which relies on the proper modification of wavelet coefficients. The wavelet shrinkage method, for instance, tries to reduce speckle noise by reducing the coefficients that correspond to speckle noise [12]. And, in addition to reducing noise, the wavelet shrinkage and contrast enhancement (WSCE) method tries to enhance the contrast by amplifying the wavelet coefficients that correspond to the edges [13]. Both these methods assume that the signal energy is larger than the noise energy in all wavelet levels. Then, by thresholding the wavelet coefficients, the two methods try to discriminate the signal and noise in the detail sub-bands at each wavelet level. In higher wavelet levels of fine resolution, however, the SNR of ultrasound images is too low to enable the signal to be separated from the noise by the thresholding of the wavelet coefficients (refer to Fig.3). Hence, depending on the adopted threshold value in each level, the signal can be reduced together with noise or the noise can be amplified with the signal.

As mentioned above, the simultaneous approach to reducing the speckle noise and enhancing edge features is still a challenging problem because the conventional thresholding scheme is not good enough to discriminate the signal from the noise. Moreover, existing methods do not consider the subjective quality and tend to produce images that look artificial. We therefore develop an algorithm that efficiently improves ultrasound images by alleviating speckle noise while

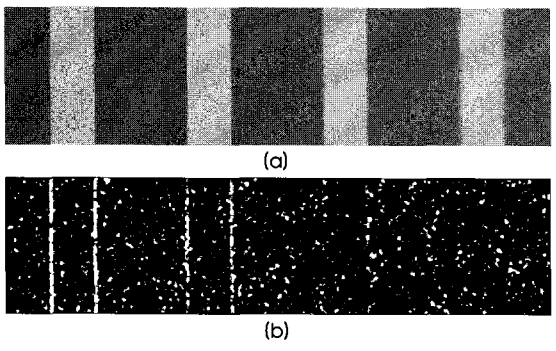

Fig. 2. (a) A phantom image with edges of various transition widths and white Gaussian noise (σ=30).(b) Edges detected by the NCD-based edge detection scheme. The variance of the Gaussian noise is set to 9 and the threshold value is set to 200.

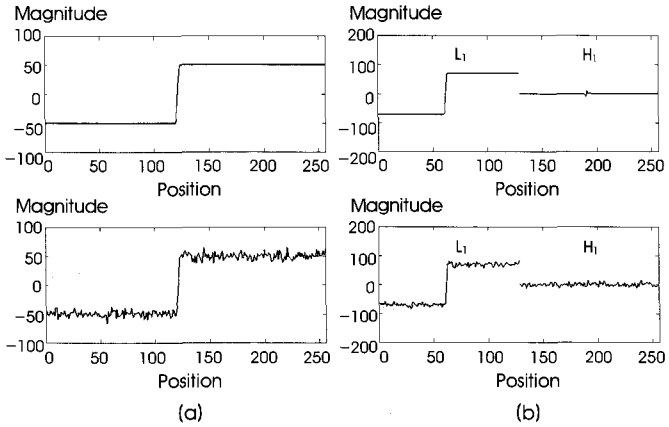

Fig. 3. (a) The original signal and its noisy signal with an SNR of 20dB. The noisy signal includes white Gaussian noise. (b) Results of a one-level wavelet transform. In the lower graph of (b), the signal information is difficult to distinguish from the noise in the first level.

enhancing edges or anatomical features; and the resultant images facilitate diagnosis. Based on a multi-resolution approach, the algorithm efficiently enhances edges of various transition widths and improves the subjective quality by properly reducing speckle noise rather than removing it.

We organize this paper as follows: In Section II, we describe the proposed algorithm. In Section II-A, we briefly review the wavelet transform and its characteristics in relation to the proposed algorithm. In Section II-B, we introduce a new gradient for efficient edge examination; the new gradient is a slightly modified version of the conventional definition of a gradient. We also explain the edge extraction procedure, which is based on a structure matrix derived from the new gradient. In Section II-C, we describe the proposed procedures for reducing the speckle and enhancing the edges. In Sections III and IV, we compare the experimental results of the proposed algorithm with the results of two other algorithms and discuss them. Finally, in Section V, we draw our conclusion.

II. PROPOSED ALGORITHM

The proposed algorithm adopts a wavelet transform based multi-resolution approach. Fig. 4 shows an overall block diagram of the proposed algorithm, which uses an N-level wavelet transform. As shown in the figure, the algorithm has two parts: the analyzing phase and the filtering phase. In the analyzing phase, edges are identified and their orientations are examined at each resolution image during the image decomposition. Thus, we can effectively divide the image into edge regions and homogeneous regions where the speckle noise is noticeable. In the filtering phase, a procedure that enhances edges in edge regions and reduces noise in homogeneous regions is sequentially applied to images with levels of resolution that range from a coarse to fine.

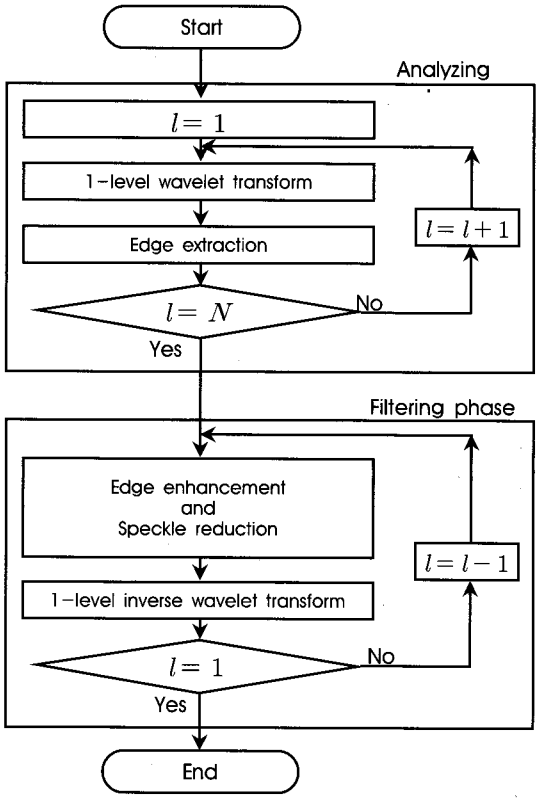

Fig. 4. Overall block diagram of the proposed algorithm

A. Wavelet transform

Noise filtering in the frequency domain can cause edge blurring because the filtering cannot be spatially adaptive. Meanwhile, filtering in the spatial domain can solve this problem by excluding edges from the filtering process. In general, the edges of an image can be easily excluded when the image resolution is unique and the SNR is high. However, because ultrasound images contain edges of various transitions with a low SNR, it may be difficult to accurately exclude edges in the spatial domain. Hence, for effective filtering of ultrasound images, we adopt a multi-resolution approach, based on a wavelet transform that simultaneously provides frequency information and spatial information.

The wavelet transform, which can decompose an image into several frequency bands by using wavelet functions and scaling functions, can be easily implemented in the digital domain by low-pass filtering, high-pass filtering, down-sampling, and up-sampling. Fig. 5 shows a couple of examples of the wavelet transform. As shown in Fig. 5(a), a one-level wavelet transform enables an original image to be decomposed into four sub-band images: LL_1 denotes a low-resolution image acquired by low-pass filtering along the x and y directions and the twofold decimation and HL_1, LH_1, and HH_1 represent the vertical, horizontal, and diagonal details, respectively. As shown in Fig. 5(b), we accomplish a two-level wavelet transform by repeating the one-level wavelet transform on the LL_1 image and decomposing the LL_1 image into LL_2, HL_2,

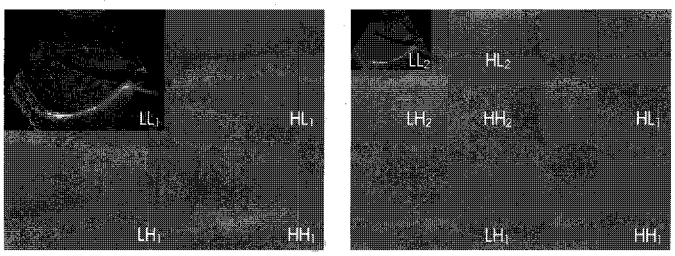

(a) (b)

Fig. 5. (a) The one-level wavelet transform. (b) The two-level wavelet transform

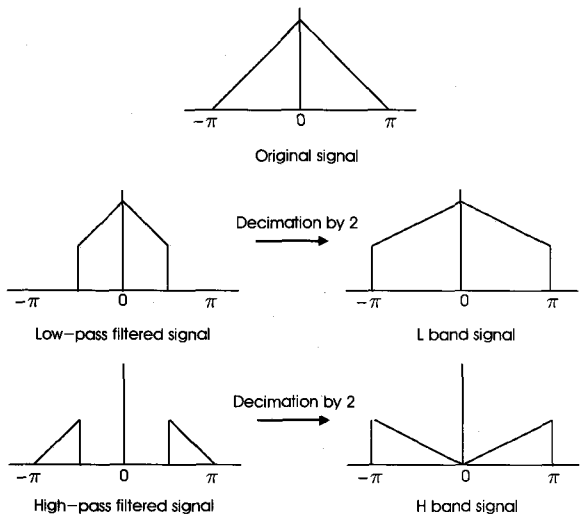

Fig. 6. Frequency spectra at the L and H bands in the one-level wavelet transform

LH_2, and HH_2. The one-level inverse wavelet transform then reconstructs the original resolution image from the four sub-band images of the first level by up-sampling and filtering. And the two-level inverse wavelet transform sequentially applies the one-level inverse wavelet transform to the four sub-band images of the second level and the four sub-band images of the first level.

We now review the frequency characteristics of the wavelet bands in the wavelet transform. For simplicity, we consider a 1-D one-level wavelet transform. Fig. 6 shows that the frequency components in the range $0 \leq \omega \leq \pi/2$ of the original signal are stretched to the range $0 \leq \omega \leq \pi$ in the L band signal. In the H band signal, on the other hand, the rest of the frequency components in the range $\pi/2 \leq \omega \leq \pi$ are inversely stretched to the range $0 \leq \omega \leq \pi$. These characteristics can be simply extended to the 2-D wavelet transform.

When we use digital filters and decimation to decompose a signal, aliasing is introduced due to non-ideal filter characteristics. The signal components affected by aliasing are mainly located near the cut-off frequency of the filters. And the aliasing is compensated and eliminated in the reconstruction procedure because of the symmetry of the quadrature mirror filters. In wavelet transform-based filtering, however, decomposed signals may be modified before the reconstruction. Hence, we cannot guarantee that the aliasing artifacts are removed in the reconstruction procedure.

B. Analyzing phase

For adaptive filtering, we need to determine the edge points and acquire information regarding their positions and directions. Fig. 7 shows that wavelet domain processing is more effective for identifying various edges of different transitions than spatial domain processing. However, a method of thresholding wavelet coefficients or the Bayesian method is not good enough for identifying edges in ultrasound images of low SNR [11-19], because the magnitude of the wavelet coefficients of the edge signals is comparable to that of noise in the HL, LH, and HH band images (see Fig. 3). Meanwhile, it is known that the images of the LL bands are less affected by noise and have good spatial information. Hence, to identify edges, we analyze the LL band images at all levels of wavelet decomposition by using structural information.

An anisotropic diffusion model is effective for identifying edges. Hence, in analyzing the images of the LL bands, we use a nonlinear anisotropic coherent diffusion model based on a structure matrix [7,8]. The structure matrix at each pixel, $\mathbf{J}_\rho$, can be written as

$$\begin{aligned} \mathbf{J}_\rho(\nabla I) &= K_\rho * (\nabla I \otimes \nabla I) \\ &= K_\rho * (\nabla I \nabla I^T) \text{ for } \rho \geq 0, \end{aligned} \tag{1}$$

where ∇I denotes the gradient at each pixel, the symbol '$\otimes$' denotes the tensor product, and the symbol '*' denotes the convolution operator. Gaussian convolution kernel, K_ρ, is expressed as follows:

$$K_\rho(x, y) = (2\pi\rho^2)^{-1} \cdot \exp\left(-\frac{x^2+y^2}{2\rho^2}\right). \tag{2}$$

Equation (1) can be rewritten as

$$\mathbf{J}_\rho(\nabla I) = K_\rho * \begin{pmatrix} I_x \\ I_y \end{pmatrix} (I_x \quad I_y) = \begin{pmatrix} K_\rho * I_x^2 & K_\rho * I_x I_y \\ K_\rho * I_x I_y & K_\rho * I_y^2 \end{pmatrix}. \tag{3}$$

The eigenvalue decomposition of the term on the right side of (3) results in the following equation:

$$\mathbf{J}_\rho(\nabla I) = (\omega_1 \quad \omega_2) \begin{pmatrix} \mu_1 & 0 \\ 0 & \mu_2 \end{pmatrix} \begin{pmatrix} \omega_1^{\mathrm{T}} \\ \omega_2^{\mathrm{T}} \end{pmatrix}, \tag{4}$$

where the eigenvector ω_1 represents the direction with the maximum variation and the eigenvector ω_2 represents the direction with the minimum variation and the eigenvalues μ_1 and μ_2 denote the magnitudes of ω_1 and ω_2.

A pixel with an anisotropic nature has a large difference between its two eigenvalues and is likely to be located on an

edge. In this case, we can consider the edge direction (or the tangential direction of the edge) to be the direction of the eigenvector with the smaller eigenvalue. In contrast, a pixel with an isotropic nature is likely to be located in a homogeneous region where speckle noise is dominant. Hence, if the difference between a pixel's two eigenvalues is small, the pixel is considered speckle noise. From eigen analysis of the LL_i band image, we can therefore obtain the edge map $E_l(x, y)$ as follows:

$$E_l(x,y)=\begin{cases}1 & ||\mu_1|-|\mu_2|| > Th_l\,,\\ 0 & \text{elsewhere}\,,\end{cases} \tag{5}$$

where $l= 1, \cdots, N$ for an N-level wavelet transform.

For a phantom image with edges of various transition widths, as shown in Fig. 2(a), we use the diffusion model described above to obtain edge maps for the images of the LL_1, LL_2, and LL_3 bands. Fig. 7 shows the detected edges for the three bands. In contrast to the NCD-based edge detection scheme, which is shown in Fig. 2(b), edges of various transitions are well determined for the images of the three bands as shown in Fig. 7.

To obtain the structure matrix, we need the gradient at every point. The matrix is usually obtained with the following definitions:

$$\begin{aligned} I_x(x,y) &= \{I(x+1,y)-I(x-1,y)\}/2,\\ I_y(x,y) &= \{I(x,y+1)-I(x,y-1)\}/2,\end{aligned} \tag{6}$$

where $I(x, y)$ represents the intensity value at point (x, y) in an image; and I_x and I_y denote the corresponding gradient values along the x and y directions, respectively. However, since (6) produces a zero gradient value for the pixel that represents a peak or a valley, that pixel is not classified as an edge pixel; though the exclusion of such pixels is undesirable for determining edge points.

A pixel in a coarser resolution image reveals the structural information of several pixels in a fine resolution image. Hence, for edge enhancement, the accurate determination of the location and direction of an edge is more important in coarser resolution images than in the fine resolution image. Hence, we modify the definition of a gradient as follows:

$$\begin{aligned} I_x(x,y) &= sing_x\cdot\{|I(x+1,y)-I(x,y)|+|I(x,y)-I(x-1,y)|\}/2,\\ I_y(x,y) &= sing_y\cdot\{|I(x,y+1)-I(x,y)|+|I(x,y)-I(x,y-1)|\}/2,\\ sign_x &= \frac{I(x+1,y)-I(x-1,y)+\epsilon_x}{|I(x+1,y)-I(x-1,y)+\epsilon_x|},\ \epsilon_x=(I(x,y)-I(x-1,y)+\epsilon)\epsilon,\\ sign_y &= \frac{I(x,y+1)-I(x,y-1)+\epsilon_y}{|I(x,y+1)-I(x,y-1)+\epsilon_y|},\ \epsilon_y=(I(x,y)-I(x,y-1)+\epsilon)\epsilon,\end{aligned} \tag{7}$$

where $sign_x$ and $sign_y$ represent the direction of conventional gradients, and ϵ_x and ϵ_y are introduced to define the sign when the point is on a peak or a valley. Note that a very small value of ϵ prevents the denominator from becoming zero for a pixel located in a homogeneous region. For a pixel residing in a monotonically decreasing or increasing area, the new definition provides the same sign and magnitude of gradients as the conventional definition. For a peak or a valley, however, the new definition still provides a non-zero magnitude, which corresponds to average intensity variation, with a proper sign.

Fig. 8 demonstrates the tangential edge direction for pixels in an LL_2 image. Fig. 8(a) shows, as expected, that the conventional method generates many wrong edge directions; in contrast, as in Fig.8(b), the proposed method provides fairly correct edge directions, even in peak or valley points.

C. Filtering phase

In the filtering phase, we perform the speckle reduction and edge enhancement at each resolution level, on the basis of the edge information obtained in the previous analyzing phase. The speckle reduction is conceptually an edge-excluded low-pass filtering procedure. The edge enhancement procedure uses directional filtering to improve edge continuity and to

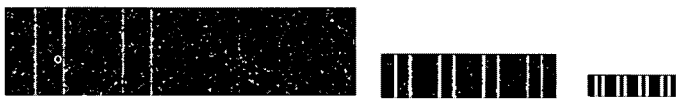

Fig. 7. The edges detected at levels LL_1, LL_2, and LL_3 with the proposed multi-resolution method. The phantom image is the same as that used in Fig. 2(a).

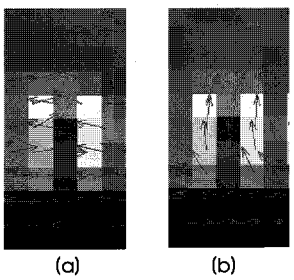

Fig. 8. Eigenvectors of the tangential direction obtained by (a) the conventional gradient calculation method and (b) the proposed method

enhance edge contrast.

We now describe the two filtering procedures in detail. With respect to the reduction of speckle noise in each level of the wavelet, speckle noise is usually modeled as multiplicative noise. In practical ultrasound images, however, speckle noise can be considered additive white noise because the images are log-compressed in a conventional ultrasound scanner. Low-pass filtering is the general method for removing the additive white noise. And it is well known that low-pass filtering can be achieved in a wavelet domain if we eliminate or properly reduce the wavelet coefficients in the HL, LH, and HH bands. Hence, by properly reducing only the wavelet coefficients that correspond to the speckle noise, we can execute edge-excluded filtering while preserving the wavelet coefficients that correspond to the edges identified in the analyzing phase. Thus, in contrast to convolution-based filtering, wavelet domain filtering can easily exclude edges from low-pass filtering.

Physicians often dislike ultrasound images with considerably lowered speckle noise. Hence, we properly reduce, rather than completely eliminate, the wavelet coefficients that correspond to speckle noise. For the low-pass filtering, we apply the following reduction ratio $R_l(x, y)$ in relation to level l:

$$R_l(x,y) = \begin{cases} 1 & \text{if } E_l(x,y) = 1, \\ k_l & \text{otherwise}, \end{cases} \tag{8}$$

where k_l denotes the reduction ratio and has a constant value. The speckle reduction ratios are heuristically determined on the basis of subjective quality tests. Fig. 9(a) shows the 1-D frequency response at each level of a three-level wavelet transform. By properly selecting reduction ratios according to the level, we can easily apply various filters. Fig.9(b) shows the frequency response of the low-pass filter by using the reduction ratios adopted in this paper. Because the speckle noise components that are decomposed into high levels of coarse resolution generate more annoying noise patterns than those that are decomposed into low levels of fine resolution, we attenuate the components in the third level more than the components in the other levels.

For the edge enhancement in the second procedure, we perform a directional filtering process, which consists of directional smoothing along the tangential direction of an edge and directional sharpening along its normal direction. The directional filtering improves the edge continuity and the directional sharpening enhances the contrast. When enhancing the contrast, we should prevent the noise from being amplified. We may therefore need to perform the edge enhancement only in the LL band images at all levels of wavelet decomposition where the images are less affected by noise. During the edge enhancement, however, undesirable aliasing artifacts can be introduced if the filtering is applied only to the L band. As mentioned in Section II-A, we cannot compensate for, or eliminate, the aliasing that comes from non-ideal short-tap wavelet filters or the corresponding artifacts if the frequency characteristic that corresponds to our filtering process is not symmetric between the L and H bands. To alleviate this problem, we perform the filtering in both the L and H bands, to ensure the symmetry of the resulting frequency characteristics of the two filtering processes.

Fig. 10 shows that the edge sharpening process has a symmetric frequency characteristic. If the same filter kernel is applied to both the L and H bands in the 1-D one-level wavelet transform domain, respectively, the frequency characteristics in the L and H bands can be represented as in Fig. 10(a) and (b), respectively. Because the frequency spectrum in the H band is a reversely stretched version of the corresponding range of the signal spectrum (see Fig. 6), the sharpening kernels applied to the L and H band signals can be interpreted as a sharpening filter, as illustrated in Fig. 10(c), for the reconstructed signal. Note in the graph that the frequency response

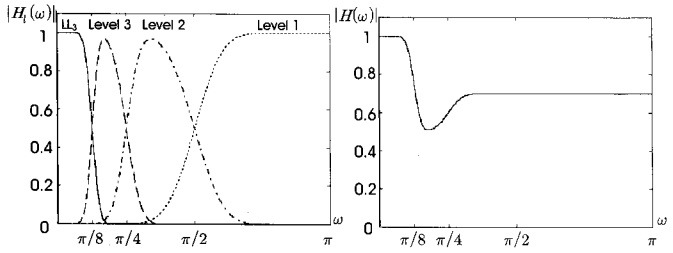

Fig. 9. (a) One-dimensional frequency response at each level of the three-level wavelet transform. (b) One-dimensional frequency response of a speckle reduction filter. The filtering is performed by weighting the wavelet coefficients in the third, second, and first levels with different weighting factors. In these graphs, the Daubechies' Symmlet 8 is used for the wavelet transform.

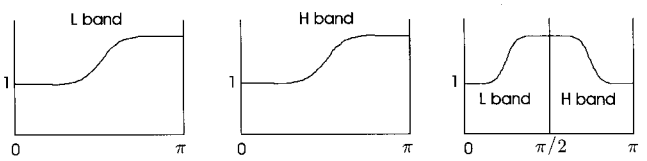

Fig. 10. Frequency characteristics of a sharpening kernel in (a) the L band and (b) the H band of the 1-D one-level wavelet domain. (c) The frequency characteristic corresponding to the reconstructed signal.

that corresponds to this filter process is symmetric at $\omega = \pi/2$. Hence, we can expect that the aliasing artifact is negligible after the filtering.

The smoothing process in the wavelet transform domain can be interpreted in the same manner as in the sharpening process. On the basis of this observation, we perform the same directional filtering in the four bands of LL, HL, LH, and HH rather than only in the LL band, thereby reducing the aliasing artifacts due to filtering. Note that we sequentially repeat this filtering process starting from the highest wavelet level.

Fig. 11 illustrates the overall directional filtering process. The two eigenvectors of a pixel on an edge represent the tangential and normal directions of the edge. By applying three-tap smoothing and sharpening kernels, namely $[w_t \ 1\text{-}2 \ w_t \ w_t]$ and $[-w_n \ 1+2w_n \ w_n]$, along the tangential and normal directions, respectively, we can rewrite the overall filtering procedure as

$$I' = (1-2w_t+2w_n)\cdot I + w_t\cdot(I_{t1}+I_{t2}) - w_n\cdot(I_{n1}+I_{n2}), \tag{9}$$

where I is the original pixel value at point P_0 in the image, I' is filtered value of the original pixel, and I_{t1}, I_{t2}, I_{n1}, and I_{n2} denote the pixel values at points P_{t1}, P_{t2}, P_{n1}, and P_{n2}, respectively. Note that by changing the filter coefficients w_t and w_n we can adjust the degree of filtering. For example, if we use a large w_t and w_n, we can achieve strong filtering.

When calculating the pixel values I_{t1}, I_{t2}, I_{n1}, and I_{n2} for the filtering, we need an interpolation procedure in the wavelet transform band. For linear interpolation in the L band, we use a triangular low-pass filtering kernel. For the H band, we use its high-pass filtering version for the interpolation because the frequency components are inversely distributed as shown in Fig. 6. If we consider 2-D interpolation in the LH band, for example, the low-pass filtering kernel is to be applied for interpolation along the x direction and its corresponding high-pass filtering kernel along the y direction.

Because a point on an edge has an anisotropic diffusion nature, the difference between two eigenvalues becomes large. By normalizing the difference with the sum of two eigenvalues, we can represent the degree of diffusion anisotropy with values between 0 and 1, regardless of their magnitudes. Accordingly, we set the filter coefficients by using the following equations so that stronger filtering kernels may be applied for a more clearly defined edge:

$$w_t = w_{t,\max}\left(\frac{\mu_1-\mu_2}{\mu_1+\mu_2}\right),$$
$$w_n = w_{n,\max}\left(\frac{\mu_1-\mu_2}{\mu_1+\mu_2}\right), \tag{10}$$

where $w_{t,\max}$ and $w_{n,\max}$ denote the maximum values of w_t and w_n, respectively.

III. EXPERIMENTAL RESULTS

We compare the proposed algorithm with two existing algorithms that are the NCD model-based method [8] and the WSCE method [13]. For the experimental images, we use scan-converted ultrasound images acquired from a convex or a linear probe. We empirically choose all the parameters needed for the experiment. First, we set the level of the wavelet transform to 3. We then set the three thresholding parameters

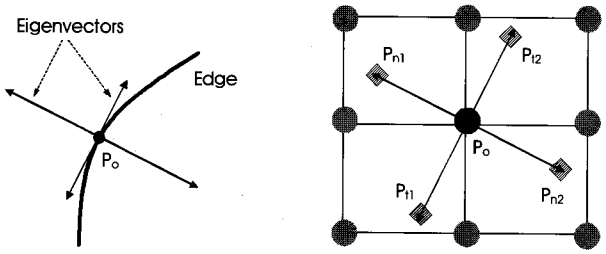

Fig. 11. Directional filtering

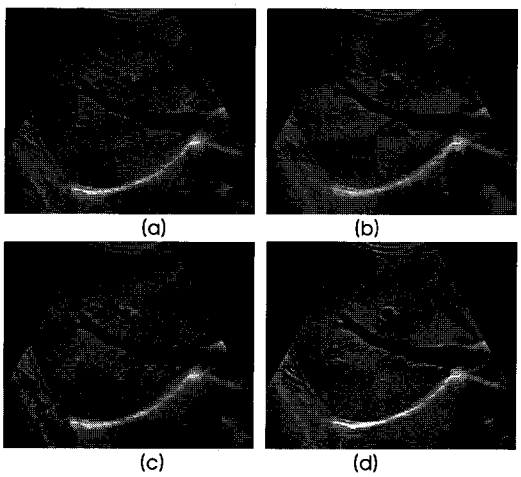

Fig. 12. Experimental results for a liver image. (a) Original image, and (b), (c), (d) the images processed by using the NCD model-based, WSCE, and proposed algorithms, respectively.

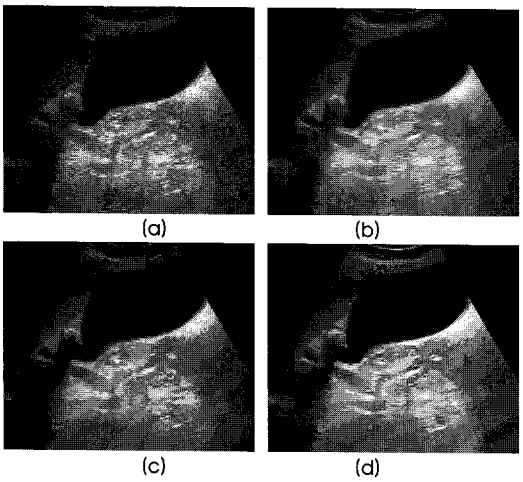

Fig. 13. Experimental results for a gallbladder image. (a) Original image, and (b), (c), (d) the images processed by using the NCD model-based, WSCE, and proposed algorithms, respectively.

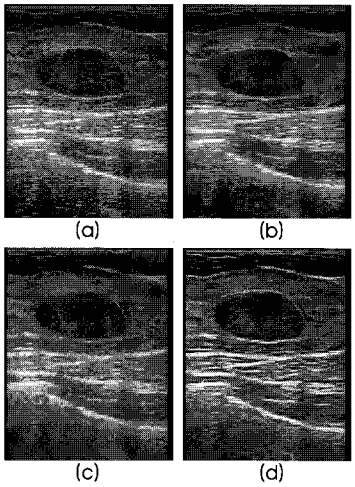

Fig. 14. Experimental results for a breast image. (a) Original image, and (b), (c), (d) the images processed by using the NCD model-based, WSCE, and proposed algorithms, respectively.

of (5), namely Th_1, Th_2, and Th_3, to 1500, 3000, and 6000, respectively. Next, we set the speckle reduction ratios for the low-pass filtering, namely k_1, k_2, and k_3 of (8), to 0.7, 0.7, and 0.5, respectively and finally we set the parameters for the directional filtering, $w_{t,\max}$ and $w_{n,\max}$, to a common value of 0.2 for all levels. For computational simplicity, we use Daubechies four-tap filters for the wavelet transform because we can hardly see any aliasing or ringing artifacts in the images due to the short tap filters.

Fig. 12 shows the experimental results for a liver image captured from a convex probe. The results of the NCD method, which are shown in Fig. 12(b), indicate enhanced structures and a significant reduction of speckle noise. But some details are lost and some details are over-enhanced. The results of the WSCE method, which are shown in Fig. 12(c), indicate that the speckle noise is reduced relatively well, but the structures are blurred and some visible artifacts are introduced. These unwanted effects occur because the thresholding technique in the wavelet shrinkage scheme reduces the sharpness of structures together with speckle noise. We note also that the images in (b) and (c) look artificial due to the speckle noise reduction. Meanwhile, Fig. 12(d) shows that the speckle noise is partially reduced in the results of the proposed algorithm, indicating that the subjective quality has not been degraded and that the structures have been enhanced without any noticeable loss or artifact. In addition, the edge orientations are maintained and the edge continuities are improved.

Fig. 13 shows the experimental results for a gallbladder image, and these results show a similar tendency to the results in Fig. 12. Notice also that the structure boundaries in Fig. 13(d) are clearer than those in Figs. 13(b) and 13(c). Fig. 14 depicts the experimental results for an image of an abnormal

Table 1. Blind test results for the subjective quality of processed images

Organ	Algorithm	Score	
		Mean	Standard deviation
Liver	NCD	1.47	0.50
	WSCE	1.53	0.50
	Proposed	3.00	0.00
Gallbladder	NCD	2.00	0.00
	WSCE	1.00	0.00
	Proposed	3.00	0.00
Breast	NCD	1.88	0.29
	WSCE	1.12	0.29
	Proposed	3.00	0.00

breast; in this case, the image was captured from a linear probe. The breast image differs from that of the liver image: that is, the breast image has fewer homogeneous regions and its edges are denser. As shown in Fig. 14(b), the NCD method reduces the speckle noise well but the image looks artificial due to blurring; in addition, some edges are lost and some are over- enhanced along the unwanted direction. The WSCE method, on the other hand, as shown in Fig. 14(c), blurs edges as well as speckle noise. The results of the proposed algorithm, which are shown in Fig. 14(d), reveal that the edges are enhanced in terms of continuity and contrast while the speckle noise is reduced.

To evaluate the performance in terms of subjective quality, we conduct blind tests with a group of 16 clinical experts. The best result is indicated by a score of 3 and the worst result by a score of 1; the final scores are averaged. The results in Table 1 demonstrate that the proposed algorithm provides the best subjective quality.

Ⅳ. DISCUSSION

In this paper, we focus on the subjective quality improvement of ultrasound images rather than the objective quality. Ultrasound images can be improved by enhancing edges and reducing speckle noise. Hence, the discrimination of edges from speckle noise is essential. As shown in the experimental results in section III, however, the NCD method cannot discriminate edges of low resolution from speckle noise. As a result, edges are blurred. The WSCE method is neither good enough for discriminating wavelet coefficients of edges from those of speckle noise. Thus it also blurs edges while remaining speckle noise. Moreover, the method introduces noticeable artifact caused from improper modification of wavelet coefficients. Meanwhile, the proposed algorithm can extract appropriate edges in the LL bands of different resolutions in the wavelet transform. As a result, unwanted blurring of edges is prohibited. The algorithm enhances the properly selected edges in terms of continuity and contrast by using directional filtering.

Existing methods focus on speckle noise elimination without considering the subjective image quality. Thus, processed images look artificial. Meanwhile, the proposed algorithm mainly reduces annoying speckle patterns rather than speckle noise, thereby improves the subjective quality. It should be noted in Table 1 that the proposed algorithm scores the best for all images, because it provides comfortable images to clinical experts by properly enhancing edges and reducing speckle noise with no loss of details and no noticeable artifacts.

On the other hand, the proposed algorithm requires several parameters to be chosen manually. However, since ultrasound image characteristics are very similar for a given organ, we can use the same parameters once they are determined.

Ⅴ. CONCLUSION

We present an ultrasound image enhancement algorithm based on a wavelet transform. In ultrasound images, edges have various transitions because of changes in resolution along the depth axis. We therefore adopted a multi-resolution approach to effectively determine the edges of various transitions. In ultrasound images with a low SNR, the speckle energy is comparable to the signal energy in a wide range of frequency bands. Thus, it is not easy to discriminate speckle noise from the signal if we use only the magnitude statistics of the wavelet coefficients of decomposed images. In the proposed algorithm, to effectively discriminate speckle from the signal, we obtain the structural information from wavelet-decomposed LL band images by performing eigen-analysis at each wavelet level. On the basis of the structural information, we can then adaptively apply directional filtering and speckle reduction procedures to LL, LH, HL, and HH band images in all the wavelet levels. The experimental results show that the proposed algorithm considerably improves the subjective image quality without generating any noticeable artifacts, and provides better performance than the existing representative enhancement schemes. On a PC with a Pentium IV 2.8GHz CPU and 1GB memory, the computational time for an image of 512 × 440 is about 40ms, which is considered adequate for a real-time application.

ACKNOWLEDGMENT

The authors thank Medison R&D (Seoul, Korea) for helpful discussions and the supply of materials.

REFERENCES

[1] Macovski, *Medical Imaging Systems*, Prentice-Hall, 1983.

[2] J. U. Quistgaard, "Signal acquisition and processing in medical diagnostic ultrasound," *IEEE Signal Processing Magazine.*, vol. 14, pp. 67-74, 1997.

[3] P. N. T. Wells, "Ultrasonic imaging of the human body," *Reports on Progress in Physics.*, vol. 62, pp. 671-722, 1995.

[4] A. K. Jain, *Fundamentals of Digital Image Processing.* Englewood Cliffs, NJ: Prentice-Hall, 1989.

[5] T. Loupas, W. N. Mcdicken, and P. L. Allan, "An adaptive weighted median filter for speckle suppression in medical ultrasonic images," *IEEE Trans. Circuits Syst.*, vol. 36, pp. 129-135, 1989.

[6] J. C. Bamber and C. Daft, "Adaptive filtering for reduction of speckle in ultrasonic pulse-echo images," *Ultrasonics.*, pp. 41-44, 1986.

[7] J. Weickert, "Multiscale texture enhancement," in *Computer Analysis of Images and Patterns*; *Lecture Notes in Computer Science*, vol. 970, *Springer*, pp. 230-237, 1995.

[8] K. Z. Abd-Elmoniem, A. M. Youssef, and Y. M. Kadah, "Real-time speckle reduction and coherence enhancement in ultrasound imaging via nonlinear anisotropic diffusion," *IEEE Trans. Biomedical Engineering.*, vol. 49, no. 9, pp. 997-1014, 2002.

[9] M. M. Goodsitt, P. L. Carson, S. Witt, D. L. Hykes, and J. M. Kofler, Jr., "Real-time B-mode ultrasound quality control test procedures: Report of AAPM ultrasound task group no. 1," *Med. Phys.*, vol. 25, no. 8, pp. 1385-1406, 1998.

[10] N. M. Gibson, N. J. Dudley, and K. Griffith, "A computerized quality control testing system for B-mode ultrasound," *Ultrasound in Med. & Biol.*, vol. 27, no. 12, pp. 1697-1711, 2001.

[11] R. M. Rao and A. S. Bopardikar, *Wavelet Transforms: Introduction to Theory and Applications.*, Addison Wesley Publications, 1998.

[12] D. L. Donoho, "De-noising by soft-thresholding," *IEEE Trans. Information theory.*, vol. 41, no. 3, pp. 613-627, 1995.

[13] X. Zong, A. F. Laine, and E. A. Geiser, "Speckle reduction and contrast enhancement of echocardiogram via multiscale Nonlinear Processing," *IEEE Trans. Med. Imag.*, vol. 17, 1998.

[14] Q. Zhou, L. Liu, D. Zhang, and Z. Bian, "Denoise and contrast enhancement of ultrasound speckle image based on wavelet," in *Proc. International Conference on Signal Processing.*, 2002, pp. 1500-1503.

[15] A. Achim, A. Bezerianos, and P. Tsakalides, "Novel Bayesian multiscale method for speckle removal in medical ultrasound images," *IEEE Trans. Med. Imag.*, vol. 20, no. 8, pp. 772-783, 2001.

[16] X. Hao, S. Gao, and X. Gao, "A novel multiscale nonlinear thresholding method for ultrasonic speckle suppressing," *IEEE Trans. Med. Imag.*, vol. 18, no. 9, pp. 787-794, 1999.

[17] A. Laine, J. Fan, and W. Yang, "Wavelets for contrast enhancement of digital mammography," *IEEE Eng. Med. Biol.*, pp. 536-550, 1995.

[18] P. Sakellaropoulos, L. Costaridou, and G. Panayiotakis, "A wavelet-based spatially adaptive method for mammographic contrast enhancement," *Phys. Med. Biol.*, vol. 48, pp. 787-803, 2003.

[19] Y. Xu, J. B. Weaver, D. M. Healy, and J. Lu, "Wavelet transform domain filters: a spatially selective noise filtration technique," *IEEE Trans. Image Processing.*, vol. 3, no. 6, pp. 747-758, 1994.

[20] W H. Press, S. A. Teukolsky, W. T. Vetterling, and B. P. Flannery, *Numerical recipes in C - The art of scientific computing*, Cambridge University press, pp. 463-469.